A Modular Approach to Model Oscillating Control Surfaces using Navier-Stokes Equations

Guru P. Guruswamy, guru.p.guruswamy@nasa.gov
Fundamental Modeling and Simulation Branch
NASA Advanced Supercomputing Division, Ames Research Center Moffett Field, CA

ABSTRACT

A modular procedure is presented to simulate moving control surfaces within an overset grid environment using the Navier-Stokes equations. Gaps are modeled by locally shearing the wing grids instead of using separate grids to model gaps. Grid movements for control surfaces are defined through a separate module, which is driven by an external grid generation tool. Results are demonstrated for a wing with a part-span control surface. Grids for the test case are determined from grid sensitivity studies. Steady and unsteady pressures are validated with wind tunnel data.

INTRODUCTION

The use of active controls is becoming more important for modern aerospace configurations. [1] Efforts to reduce the vibrations of helicopter blades with use of active-controls are in progress [2]. Modeling oscillating control surfaces using linear aerodynamic theory is well established. However, higher-fidelity methods are needed to account for nonlinear effects, such as those that occur in transonic flow [3]. The aeroelastic responses of a wing with an oscillating control surface, computed using transonic small perturbation (TSP) theory, have been shown to cause important transonic flow effects [4] such as a reversal of control surface effectiveness that occurs as the shock wave crosses the hinge line. In order to account for flow complexities such as blade-vortex interactions of rotor blades [5] higher-fidelity methods based on the Navier-Stokes equations are used.

Reference 6 presents a procedure that uses the Navier-Stokes equations with moving-sheared grids and demonstrates up to 8 degrees of control-surface deflection, using a single grid. Later, this procedure was extended to accommodate larger amplitudes, based on sliding grid zones [7]. The sheared grid method implemented in the Euler/Navier-Stokes-based aeroelastic code ENSAERO [6] was successfully applied to active control design by industry [8].

Recently several papers [9, 10, 11, 12] have been published that present results for oscillating control surfaces using the Reynolds Averaged Navier-Stokes (RANS) equations. References 9 and 10 report 2-D cases using an approach of filling gaps with overset grids. Reference 9 compares integrated forces with an experiment at low oscillating frequencies whereas Ref. 10 reports parametric studies but with no validation. Reference 11 reports results for a 3D case by modeling the gap region with a smeared grid and compares force results with an experiment only at the mid-span of the flap. In Ref. 11 the grid is deformed to match the control surface deflections only at the section where the measurements are made without explicitly modeling the gap as in Ref. 6. Computations using overset grids are reported in Ref. 12 for a case by adding a moving control surface to an existing blade but with no validation either with an experiment or another computation.

In Ref. 13 an oscillating control surface was simulated using the RANS-based OVERFLOW code [14] using overset grids in gaps and was validated with experiment for integrated air loads. Ref. 13 reports significant differences between computations and measurements, particularly for flap moments. While the approach presented in Ref. 13 promises to be accurate, a promise that has yet to be realized in such quantities as unsteady surface pressures, it also requires more grid points and a more complicated grid generation process. Time step restrictions associated with tightly spaced grid points in gaps can also be an issue with this approach.

As an alternate approach the present work presents a sheared grid capability [6] embedded as a module into the overset-grid-based OVERFLOW code. The shearing grid approach has been successfully implemented in using patched grids [15]. In this approach the grid at the control surface gap has the same topology as the grid for un-

Presented at the Fifth Decennial AHS Aeromechanics Specialists' Conference, San Francisco, CA, January 22-24, 2014.

deflected control surface. Control surface deflections are modeled by shearing the grid at the gap. Sheared grids produce accurate results for moving control surfaces [6, 15] and can be numerically more efficient than methods that use overset grids to model small gap, which are common when active control surfaces are used. Since the gaps size and control surface deflections are assumed to be small flow through conditions for grid points in the gap are not applied.

This work focuses on implementing and validating the sheared grid module for use with overset grids. In addition, this effort makes progress towards providing an efficient and robust high-fidelity analysis tool for designing active controls, particularly for the transonic regime. The approach is validated for a wing with part span control surfaces using unsteady pressure results from an experiment performed at the NASA Langley Research Center [16]. The test is commonly known as the BACT (Benchmark Active Controls Technology) test. None of the other recent papers [9, 10, 11, 12, 13] include validation of unsteady-surface pressures needed before validating integrated forces [13]. In addition, Refs. 9 to 13 compare only time responses with experiment that may be prone to uncertainties. The strongly preferred method in the fixed wing community [17] is to compare time integrated Fourier coefficients. This approach eliminates the effect of start times. In this work, Fourier coefficients are compared with the experiment.

APPROACH

In this paper, the RANS equations [18] are numerically solved using the Pulliam-Chaussee diagonal form of the Beam-Warming central difference algorithm [19], along with the one-equation Spalart-Allmaras turbulence model [20]. The solutions are computed using the OVERFLOW code [14], which is based on an overset grid system. The second-order spatial and temporal accuracy options available in the 2.2g version of OVERFLOW are used throughout this analysis.

In the current version of OVERFLOW, control surface motions are prescribed externally [13] and the flow solver needs to pause while getting the deflection input. In this work, the shearing grid capability is embedded within the OVERFLOW code to avoid the computer overhead time associated with pausing for data transfers. Modularity is maintained by communicating data between grid generator and flow solver through internal input/output logic. A flow diagram of the modular approach is shown in Fig. 2. Grids are generated on the fly using a grid generation subroutine. This will facilitate embedding an active control module [5, 8] in OVERFLOW.

The solid surface for the wing with a control surface is shown in Fig. 1 along with two cutting planes. One cut shows the grid in a constant span plane and the other shows the grid along the span.

The moving control surface grid is generated using the following equation. The control surface deflection angle in degrees at a given time *t* is defined as

$$\delta = \delta_{0} + \delta_{\beta} \sin(\omega t) \qquad (1)$$

where δ_0 and δ_β are the mean and maximum amplitude of the oscillatory control surface deflections in degrees, respectively. The ω and t parameters are circular frequency of the control surface oscillation in radians per sec and time in sec, respectively. All unsteady components are scaled with δ_β converted to radians.

Once δ is known the shearing displacements of grid points due to control surface motion are computed for $x > x_c$ using

$$\Delta_x = x - (x-x_c) \cos(\delta) \qquad (2a)$$

$$\Delta_z = z - (x-x_c) \sin(\delta) \qquad (2b)$$

where x_c is the x location of control surface leading edge. The surface displacements are applied to shear the near body (NB) grid. In the normal direction the shearing is linearly decayed to zero up to about 50% chord length from the surface. The x-ray box [14] in the overset grid is placed such that there are no interpolations between the moving NB grid points and the background (BG) grid. This will avoid having to re-compute interpolation coefficients every time step and save computational time.

In the spanwise direction displacements are linearly increased from zero at the beginning to full value at the end of each gap. The process shown in Fig. 2 deals with volume meshing and flow solution steps.

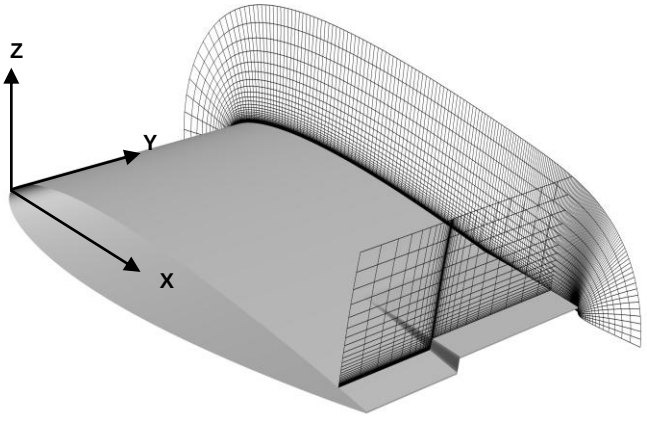

Fig. 1 Typical sheared grid for part-span control surface.

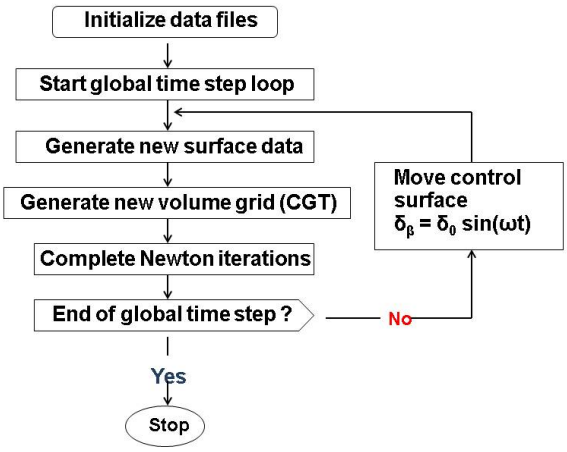

Fig. 2 Solution process.

Moving Grid Module

In Ref. 21 a wing with a full-span moving control surface was modeled using a single grid and moving grids were directly generated by executing the Chimera Grid Generation Tool (CGT) [22] every time step**.** Direct use of the CGT tool is not feasible for present work where multi-zone grids are needed. Therefore a module that generates the moving grid is embedded into OVERFLOW.

For parallel computing grid zones in OVERFLOW are assigned to different cores by a load-balancing algorithm with no user control. In the present approach it is assumed that the complete control surface is within a single grid zone. When using the MPI [23] option of OVERFLOW, the grid zone containing the control surface is assigned to a single processor without splitting the grid. However, this limitation could be removed if an option to assign specific processors to selected grid zones, similar to that implemented in HiMAP [24], were available in OVERFLOW. Confining a shearing grid module to one zone makes all computations within that module implicit and allows larger time steps for integration. Any impact on parallel efficiency can be minimized using a node-filling algorithm successfully implemented in HiMAP [24]. The present procedure of modeling the control surface in a single zone does not have any limitations when using the shared memory OpenMP [25] option of OVERFLOW.

RESULTS

Wind Tunnel Model

In this work computations are made about the BACT wind tunnel model configuration [16] that involves a wall mounted rectangular blade with a part-span oscillating control surface. A schematic diagram of the model is shown in Fig. 3. The model measures 32 inches in span and 16 inches in chord, and is made of NACA0012 airfoil sections. The leading edge of the control surface that starts at 45% span with length 9.6 inches is located at 75% chord. From the figure in the report it is estimated that the gap is about 0.5% of chord. A total of 54 upper and lower surface pressure orifices, including 16 on the control surface, were used to measure surface pressures. The measured data are given in the form of magnitude/amplitude and phase angles of unsteady pressures. The phase angle is the difference in period between the peaks of control surface deflection and the pressure/force response. The amplitude is the absolute value of the maximum response above the time-averaged value. The magnitude and phase angles are computed by performing a Fourier analysis of the time responses.

Grid Topology

An overset grid system generated by using CGT [22] is shown in Figs. 4a, 4b and 4c. The grid has near body O-H (wrap around airfoil in x-direction and stacked spanwise in y-direction) topology for the wing and a cap grid (grids radiating from surface) for the tip. In order to facilitate communications among un-connected grid points between NB wing and cap grids, a background Cartesian box grid (BG) is used.

Since the gap in the model is very small it is not modeled in the grid. The wing surface grid is sheared by applying the displacements due to control surface deflections using Eqn. (2) and a new grid is generated.

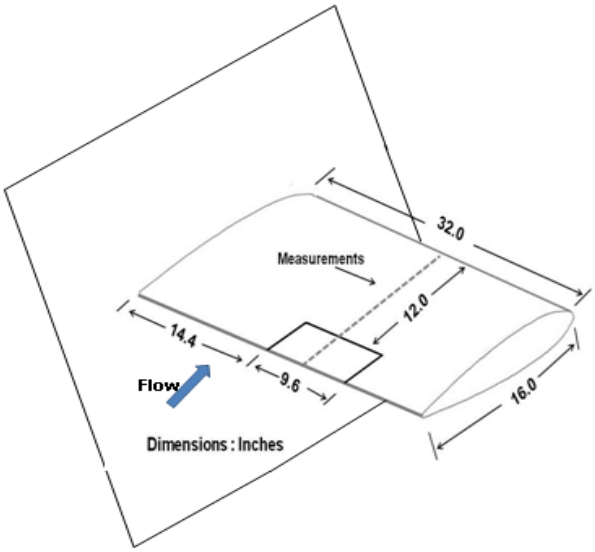

Fig. 3 Schematic diagram of the wind tunnel model.

The final grid selected is based on grid sensitivity studies for both spatial and temporal accuracies.

Grid Sensitivity Studies

A case at free stream Mach number $M_\infty = 0.77$, angle of attack $\alpha = 4.0$ deg and control surface mean deflection $\delta_0 =$

5.0 deg for which both mean steady and unsteady pressure data are available is selected for grid sensitivity studies. The associated Reynolds number Re_c based on chord (c) is 3.82 million.

First, a grid with attributes based on previous experience using the CGT tool [22] is selected. For the NB wing grid average surface grid spacing of 0.0000125c, near-body stretching factor of 1.125, average chordwise spacing of 0.005 and outer boundary (OB) grid surface location at 1.5c are selected. The grid spacing at the leading edge is about 0.0025c. With these parameters a wing grid with 403 points around the airfoil section and 60 points in the normal direction is generated using the hyperbolic grid generator [22]. A spanwise grid utilizing 95 points with grid points clustered at the control surface edges is generated. The gaps which are assumed to be of size 0.05c are modeled using 5 grid points each (see Fig 4c). Using the module available in CGT, a cap grid with 97x49 surface points and 60 points in radial direction is generated. The BG box grid has 141 points in each x and z directions and 82 points in the y direction. It has 0.1c constant spacing up to about 5c and then stretched to outer boundary located at about 18c. For this selected grid (SG) topology with 3-grids, effects of various grid attributes on sectional lift coefficient (c_l), moment coefficient about leading edge (c_m) and drag coefficient (c_d) are studied to determine the final grid.

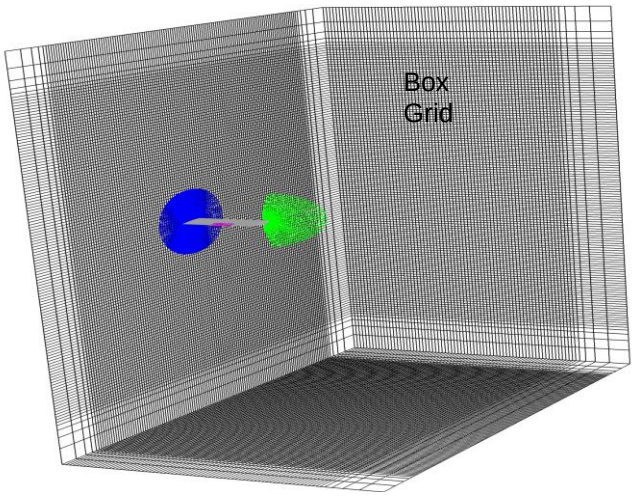

Fig. 4a Grid Topology-Near body and a portion of box grid.

Steady-flow computations at M_∞ = 0.77, α = 4.0 deg, δ_0 = 5.0 deg and Re_c = 3.82 million are performed using a variable time-step option in OVERFLOW without sub-iteration. Figures 5 and 6 show convergence histories of residuals and force coefficients, respectively. The residuals show three orders drop in about 3000 iterations whereas the force coefficients show that results converge in about 2000 iterations. The rest of the steady-state computations are made using 4000 iterations.

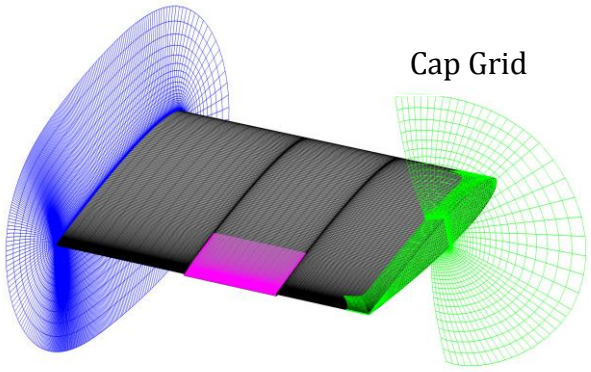

Fig. 4b Near body wing and cap grids.

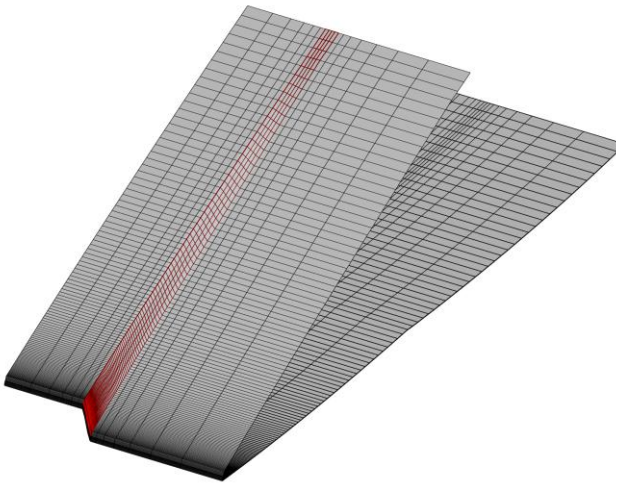

Fig. 4c Grid at gap.

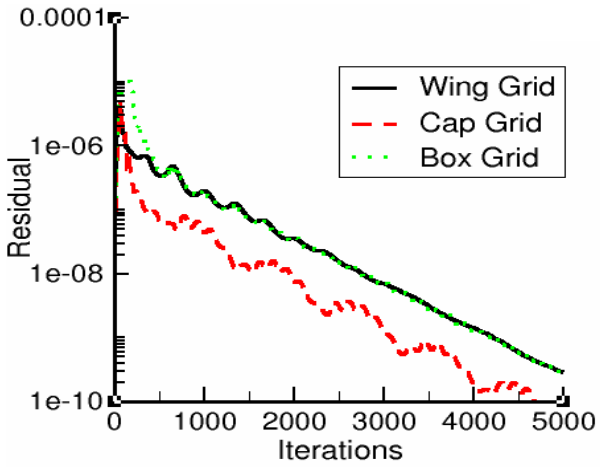

Fig. 5 Convergence residual at M_∞ = 0.77, α = 4.0, δ_0 = 5.0 deg and Re_c = 3.82 million.

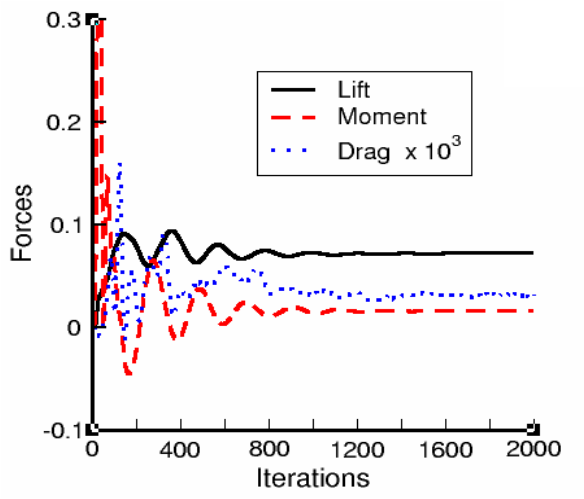

Fig. 6 Convergence steady for c_l, c_m and c_d at $M_\infty = 0.77$, $\alpha = 4.0$, $\delta_0 = 5.0$ deg and Re_c = 3.82 million.

Normal grid spacing near the surface is varied from 0.00001 to 0.00003. As observed in Fig. 7 the initially selected spacing of 0.0000125 is considered adequate since force coefficients differs less than 0.2% from values at spacing 0.00001. The surface stretching factor is varied from 1.1 to 1.3. Figure 8 shows that a surface stretching factor of 1.125 is adequate. These selected parameters yield an average y+ value of 1.09 which is considered adequate to resolve flows at the surface.

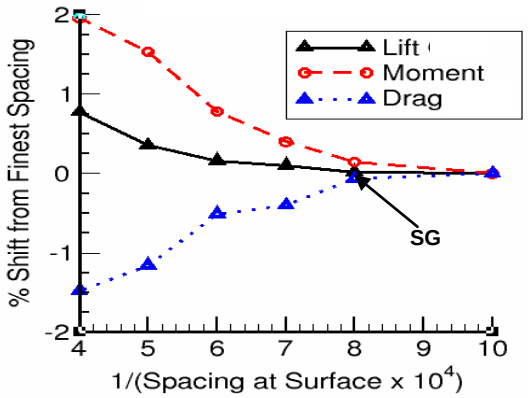

Fig. 7 Effect of normal spacing at surface on c_l, c_m and c_d at $M_\infty = 0.77$, $\alpha = 4.0$ deg , $\delta_0 = 5.0$ deg and Re_c = 3.82 million.

To study adequacy of the grid in the chordwise direction, starting from the SG grid (403 points), computations are made using a series of grids with increased spacing: double the spacing, quadruple the spacing and octuple the spacing, while keeping the remaining of the grid parameters the same. This is accomplished by modifying the selected grid (403 points) using the cubic spline interpolations in CGT [22]. Figure 9 shows the effect of grid refinement in the x-direction on c_l, c_m and c_d. As seen c_l, c_m and c_d converge for the selected grid. The chordwise spacing corresponding to 403 grid points is adequate.

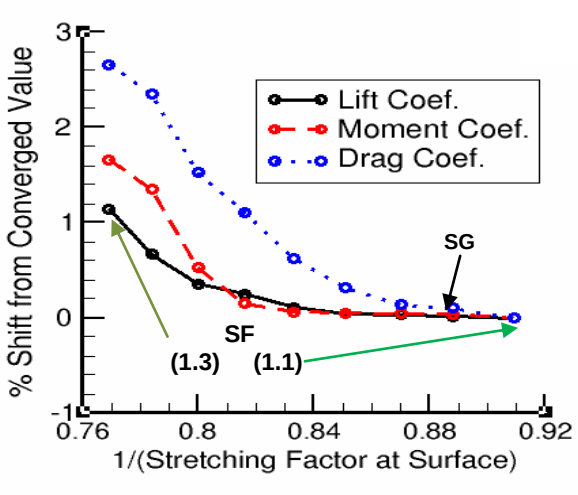

Fig. 8 Effect of normal grid stretching factor (SF) on c_l, c_m and c_d at $M_\infty = 0,.77$, $\alpha = 4.0$, $\delta_0 = 5.0$ deg and Re_c = 3.82 million.

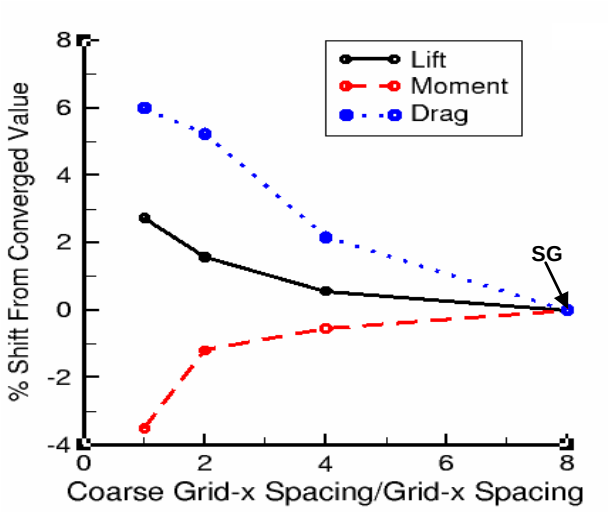

Fig. 9 Effects of chordwise spacing on c_l, c_m and c_d at $M_\infty = 0.77$, $\alpha = 4.0$, $\delta_0 = 5.0$ deg and Re_c = 3.82 million.

Using the above selected grid parameters the effect of location of the outer boundary (OB) of back ground grid is studied next. From Fig. 10 it is seen that the outer boundary of the SG grid at 18c is adequate since results does not change after about 15c.

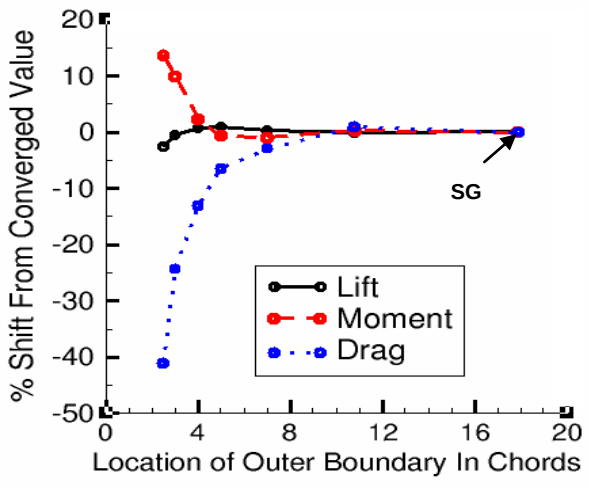

Fig. 10 Effect of outer boundary location spacing on c_l, c_m, and c_d at $M_\infty = 0.77$, $\alpha = 4.0$, $\delta_0 = 5.0$ deg and Re_c = 3.82 million.

Finally, for steady computations the effect of number of chord-wise grid lines in the gap region is studied. The average changes for 3 and 4 lines from 5 lines are 7.3% and 0.5%, respectively. The grid with 5 lines of SG is considered adequate.

Unsteady computations are performed at $M_\infty = 0.77$, $\alpha = 4.0$ deg, Re_c = 3.82 million, $k = 0.22$ and $\delta_\beta = 5.0$ deg corresponding to a test case in the experiment. Computations are performed with a variable number of steps per cycle (NSPC). It was found that NSPC = 1200 produced a stable solution without using Newton sub-iterations (NWIT). The rest of the time step convergence studies are made using NSPC = 1200.

Since Newton sub-iterations are required to maintain 2nd order time accuracy, the next study involved the variation of number of Newton sub-iterations. Computations are made for 4 cycles with increasing NWIT. Figure 11 shows the responses of c_l, c_m, and c_d for NWIT =16. The solutions during the first cycle of the computation have not achieved periodic behavior and should not be quantitatively evaluated. The solutions for cycles 2-4 are periodic. Figure 12 shows convergence plots of magnitude and phase angle of unsteady c_l with respect to increasing NWIT. Results converged at NWIT = 16. Rest of the unsteady computations are made using 4 cycles of oscillations with NSPC = 1200 and NWIT = 16.

Within the range of parameters considered for grid sensitivity studies it was observed that the outer boundary location had relatively more effect on c_l, c_m and c_d. As seen in Fig. 10, the variation is 40% for c_d for changing OB location from 2.5c to 18c. As a result, effect of outer boundary location is studied for unsteady cases.

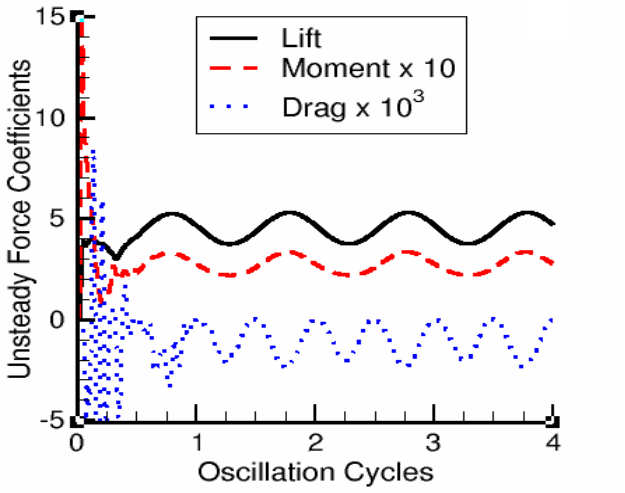

Fig. 11 Response of unsteady c_l, c_m, and c_d, at $M_\infty = 0.77$, $\alpha = 4.0$ deg, $\delta_0 = 0.0$ deg, $\delta_\beta = 5.0$ deg. k = 0.22, and Re_c = 3.82 million.

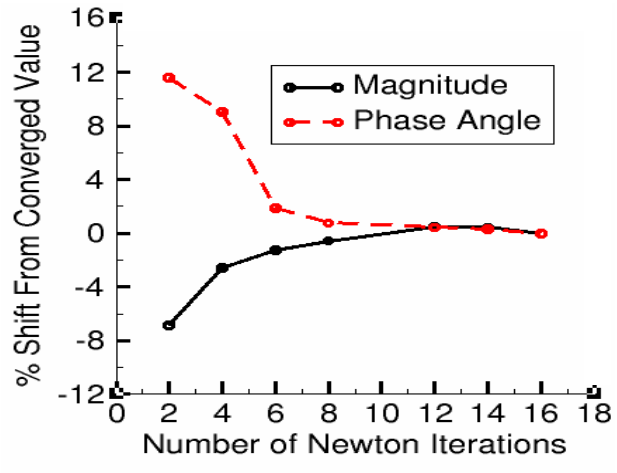

Fig. 12 Effect of number of Newton sub-iterations on magnitude and phase angles of unsteady c_l for $M_\infty = 0.77$, $\alpha = 4.0$ deg, $\delta_0 = 0.0$ deg, $\delta_\beta = 5.0$ deg, k = 0.22, and Re_c = 3.82 million.

Figure 13 shows the effect of outer boundary location on magnitude and phase angles of unsteady c_l for $M_\infty = 0.77$, $\alpha = 4.0$ deg, $\delta_0 = 0.0$ deg, $\delta_\beta = 5.0$ deg, k = 0.22, and Re_c = 3.82 million. As expected phase angle is more sensitive than magnitude. However, the changes in the values for both magnitude and phase angles are less than 0.1% from 10c to 18c.

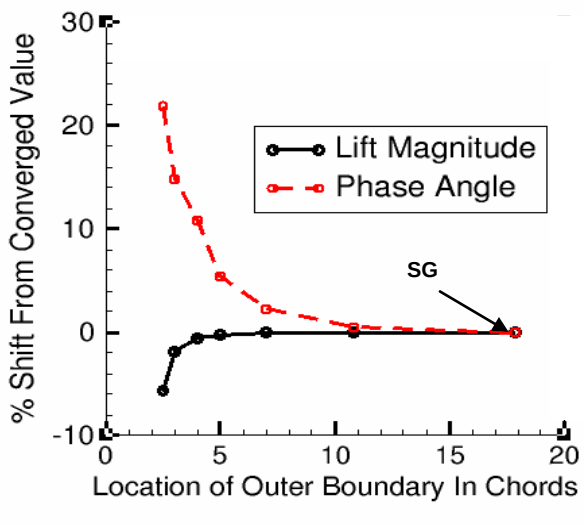

Fig. 13 Effect of outer boundary location on magnitude and phase angles of unsteady c_l for M_∞ = 0.77, α = 4.0 deg, δ_0 = 0.0 deg, δ_β = 5.0 deg, k = 0.22, and Re_c = 3.82 million.

Test Cases

Computations are made for two static cases (α = 0.0 and 4.0 deg) and two dynamic cases (k = 0.11 and 0.22) for which surface pressure data are available in public domain.

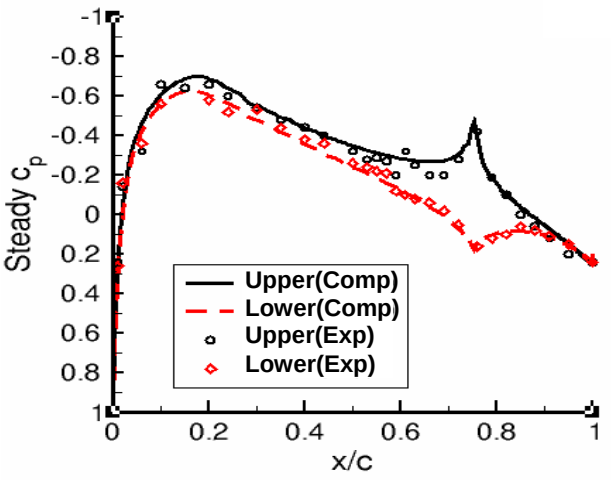

Fig. 14 Comparison between computed and measured values of steady cp for M_∞ = 0.77, α = 0.0, δ_0 = 5.0 deg and Re_c = 3.96 million.

Figure 14 shows a comparison of upper and lower surface steady c_p at M_∞ = 0.77, α = 0.0 deg, δ_0 = 5.0 deg and Re_c = 3.96 million. In general results compare well for both upper and lower surfaces. The data from experiments appears slightly scattered around x/c = 0.65 where an un-deflected spoiler (0.6 x/c 0.75) is located.

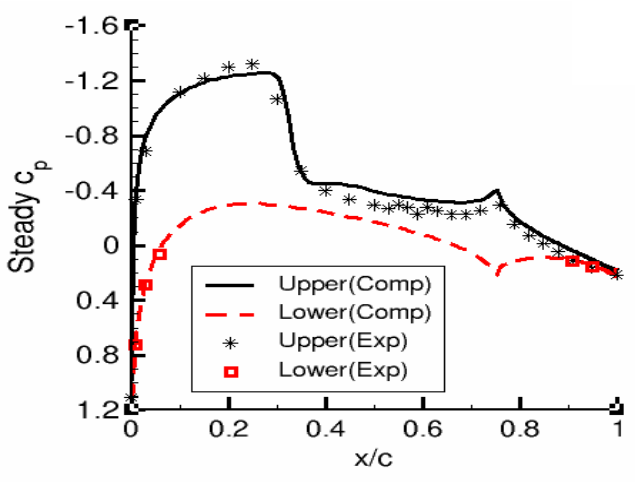

Fig. 15 Comparison between computed and measured values of steady cp for M_∞ = 0.77, α = 4.0, δ_0 = 5.0 deg and Re_c = 3.83 million.

Figure 15 shows a comparison of upper and lower surface steady c_p at M_∞ = 0.77, α = 4.0 deg, δ_0 = 5.0 deg and Re_c = 3.83 million. For this case pressures from experiment are available for all 30 upper surface pressures taps but only for 5 lower surface pressure taps. Both upper and lower surface pressures compare well between computations and experiment. Around x/c = 0.2 the experiment has slightly lower values than the computation. For x/c between 0.4 and 0.8 the experiment shows slightly higher values than the computation. For this case the computed c_l and c_m are 4 % higher and 6% lower than the measured values, respectively.

Computations are made for control surface oscillating at 5Hz (k = 0.1083) and 10 Hz (k = 0.2166). Figure 16 shows the comparison of computed results with experiment for in-phase and out-of-phase components of upper-surface oscillatory pressure at M_∞ = 0.77, α = 0.0 deg, δ_0 = 0.0 deg, δ_β = 2.0 deg, k = 0.1083, and Re_c = 3.96 million. Both components compare well with the experiment. Experiment shows a slight jump the in-phase value around x/c = 0.60 where the leading edge of the un-deflected spoiler (not modeled in this paper) is located. Possible small deflections of the spoiler, details of which are not available in the experimental report, might have caused this discrepancy.

Figure 17 shows the comparison of computed results with experiment for in-phase and out-of-phase components of upper-surface oscillatory pressure at M_∞ = 0.77, α = 4.01 deg, δ_0 = 0.0 deg, δ_β = 3.87 deg, k = 0.2166 and Re_c = 3.86 million. Both components compare well with the experiment. Computations do a good job in capturing the peaks near the shock-wave around x/c = 0.31 and at leading edge of the control surface. Experiment shows a slight jump in-phase value around x/c = 0.60 where the leading edge of the spoiler is located.

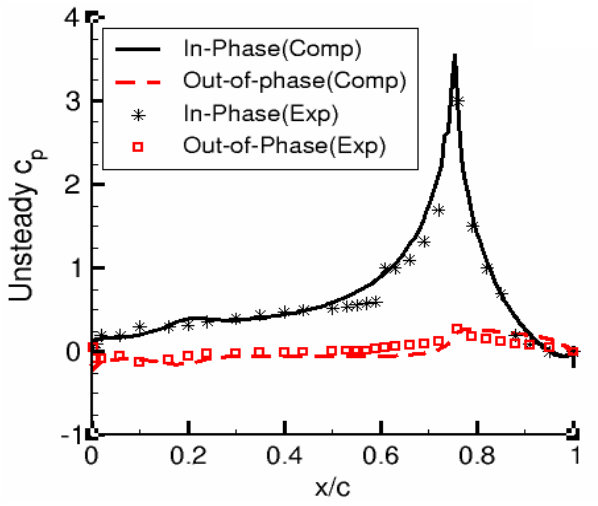

Fig. 16 Comparison between computed and measured values of in-phase and out-of-phase components of upper-surface oscillatory pressures for $M_\infty = 0.77$, $\alpha = 0.0$ deg, $k = 0.1083$, $\delta_0 = 0.0$, $\delta_\beta = 2.0$ deg and Re_c = 3.96 million.

Instantaneous surface pressure, spanwise velocity contours and chordwise density contours corresponding to maximum control surface deflection of case at 10 Hz are shown in Fig. 18. Formation of vortices at the gap can be seen in Fig. 18b.

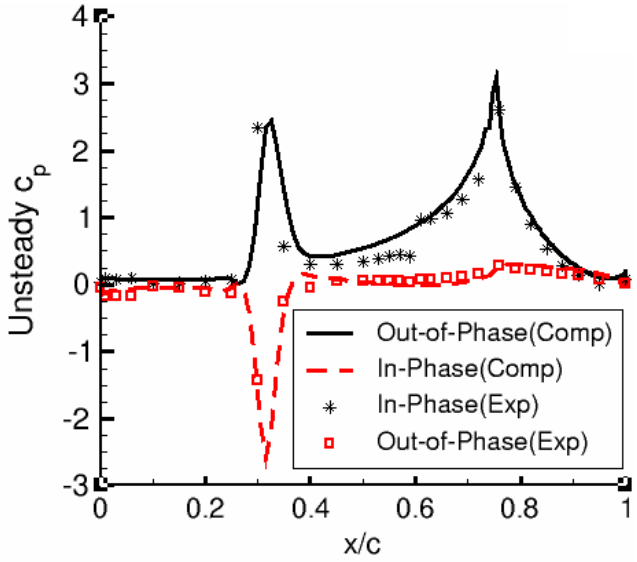

Fig. 17 Comparison between computed and measured values of in-phase and out-of-phase components of upper surface oscillatory pressures for $M_\infty = 0.77$, $\alpha = 4.01$ deg, $k = 0.2166$, $\delta_0 = 0.0$, $\delta_\beta = 3.86$ deg and Re_c = 3.86 million.

All computations are made using the OpenMP version of OVERFLOW on NASA's Pleiades super-cluster [26, 27]. The final grid with 4.21 million points needed 5.6 hrs of wall clock time per cycle (NSPC = 1200 and NWIT =16) on 20 cores. An order of magnitude increase in speed can be achieved when this calculation is extended using MPI version of OVERFLOW.

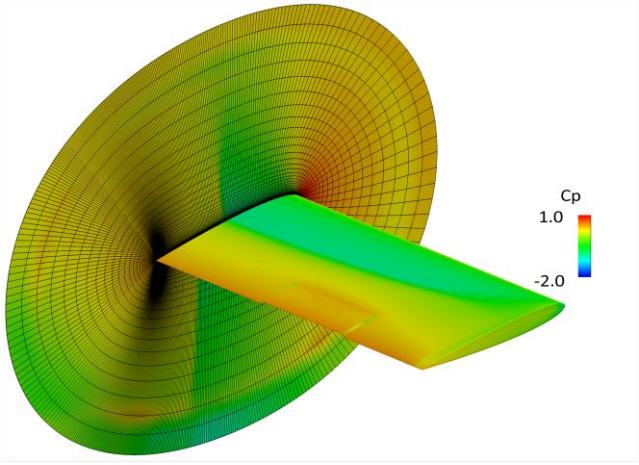

(a) Surface pressure

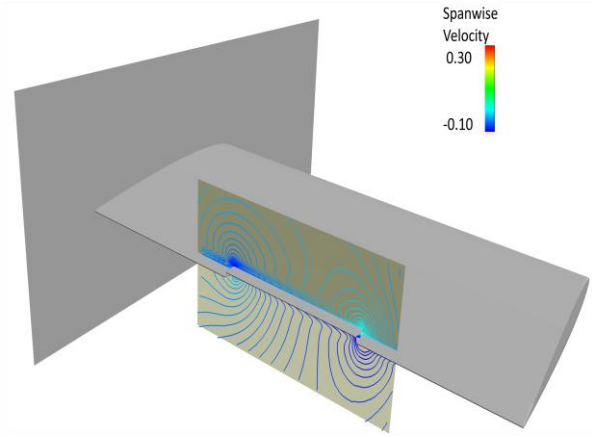

(b) Spanwise velocity contours at control surface.

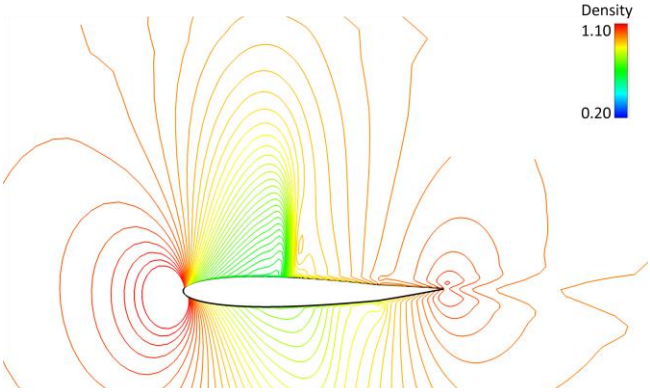

(c) Chordwise density contours at mid span of control surface.

Fig. 18 Snapshots at the peak control surface amplitude for $M_\infty = 0.77$, $\alpha = 4.01$ deg, $k = 0.2166$, $\delta_0 = 0.0$, $\delta_\beta = 3.86$ deg and Re_c = 3.86 million.

CONCLUSIONS

Computations of the flows over part-span oscillating control surfaces are performed using the Reynolds-Averaged Navier-Stokes equations. A modular embedded sheared-grid approach in the context of a general purpose overset based CFD code is used to model the oscillating control surface. The procedure is validated by comparing unsteady pressures and integrated forces with experiment. Grids are selected based on detailed grid sensitivity studies that involved effects of chordwise spacing, near surface spacing, near surface stretching factor and outer boundary location. Steady computations show that results are more sensitive to outer boundary location than other parameters. This development can be readily used for conducting simulations with active controls.

ACKNOWLEDGEMENTS

The author thanks Shishir Pandya, William Chan and Henry Lee of NASA Ames Research center (ARC) for providing help in using CGT grid tool. Consultations by Dennis Jespersen of NASA Advanced Super Computing Division (NAS) on parallel computing aspects of OVERFLOW were very helpful. Terry Holst, chief of Fundamental Modeling and Simulation Branch at NASA Ames Research Center and CFD lead of Rotary wing (RW) project, made valuable suggestions on grid refinement studies. This work was supported by RW and IRAD of NAS.

REFERENCES

1. Carey, B. "BAE Systems Develops Aircraft Active Controls Stick," Aviation International News (AIN) Online, July 10, 2012. (http://www.ainonline.com/aviation-news/2012-07-10/bae-systems-develops-civil-aircraft-active-control-stick)
2. Lau, B., Obriecht, N., Gasow, T., Hagerty, B., Cheng, K. and Sim, B., "Boeing-SMART Test Report for DARPA Helicopter Quieting Program," NASA TM 2010-216404, April 2010.
3. Mukhopadhyay, V., "Transonic Flutter Suppression Control Law Design, Analysis and Wind Tunnel Test Results," 2nd International Conference on Nonlinear Problems in Aviation and Aerospace, Daytona Beach, FL, April 1998, pp. 45-51.
4. Guruswamy, G. P., "An Integrated Approach for Active Coupling of Structures and Fluids," *AIAA J.*, Vol. 27, No. 6, June 1989, pp. 788-793.
5. Poling, D. R., Dadone, L. and Telionis, D. P., "Blade-Vortex Interaction," *AIAA J.*, Vol. 27, No. 6, June 1989, pp. 694-699.
6. Obayashi, S. and Guruswamy, G. P., "Navier-Stokes Computations for Oscillating Control Surfaces," *J. of Aircraft,* Vol. 31, No. 3, May-June 1994, pp. 631-636.
7. Klopfer, G. H. and Obayashi, S., "Virtual Zone Navier-Stokes Computations for Oscillating Control Surfaces," AIAA Paper 93-3363, 11th AIAA Computational Fluid Dynamics Conference, Orlando, FL, July 1993.
8. Yeh, D. T., "Aeroelastic Analysis of a Hinged-Flap and Control Surface Effectiveness Using the Navier-Stokes Equations," AIAA Paper 95-02263, 1995.
9. Liggett, N. and Smith, M., "Study of Gap Physics of Airfoils with Unsteady Flaps," *J. of Aircraft,* Vol. 50, No. 2, March–April 2013, pp. 643-650.
10. Liu, L., Padthe, A., Friedmann, P. P., Quon, E. and Smith, M., "Unsteady Aerodynamics of an Airfoil/Flap Combination on a Helicopter Rotor Using CFD and Approximate Methods," *J. of the American Helicopter Society*, Vol. 56, No. 3, July 2011, pp. 032003-1-032003-13.
11. Mishra, A., Sitaraman, J., Baeder, J. D. and Opoku, D. G., "Computational Investigation of Trailing Edge Flap for Control of Vibration," AIAA Paper 2007-4290, AIAA Applied Aerodynamics Conference, June 2007, Miami, FL.
12. Jain, R., Yeo, H. and Chopra, I., "Investigation of Trailing-edge Flap Gap Effects on Rotor Performance Using High-Fidelity Analysis," *J. of Aircraft,* Vol. 50, No. 1, Jan.-Feb. 2013, pp. 140-150.
13. Potsdam, M., Fulton, M. V. and Dimanlig, A., "Multidisciplinary CFD/CSD Analysis of the SMART Active Flap Rotor," Proceedings of the 66th Annual Forum of the American Helicopter Society, Phoenix, Arizona, May 2011.
14. Nichols, R. H., Tramel R. W. and Buning P. G., "Solver and Turbulence Model Upgrades to OVERFLOW2 for Unsteady and High-Speed Applications," AIAA Paper 2006-2824, AIAA 36th Fluid Dynamics Conference, San Francisco, CA, June 2006.
15. Obayashi, S., Chiu, I. and Guruswamy, G. P., "Navier-Stokes Computations on Full-Span Wing-Body Configuration with Oscillating Control Surfaces," *AIAA J.*, Vol. 32, No. 6, Nov.-Dec. 1995, pp. 1227-1233.
16. Bennett, R. M., Eckstrom, C. V., Rivera, J. A., Farmer, M. G. and Durham, M. H., "The Benchmark Aeroelastic Models Program – Description and Highlights of Initial Results," NASA TM- 107582, 1991.

17. Schuster, D. M., Heeg, J., Wieseman, C. and Chwalowski, P., "Analysis of Test Case Computations and Experiments for the Aeroelastic Prediction Workshop," AIAA Paper 2013-0788, 51st AIAA Aerospace Sciences Meeting, Jan. 2013, Grapevine, Texas.
18. Peyret, R. and Viviand, H., "Computation of Viscous Compressible Flows based on Navier-Stokes Equations," AGARD-AG-212, 1975.
19. Pulliam, T. H. and Chaussee, D. S., "A Diagonal Form of an Implicit Approximate-Factorization Algorithm," *J. of Computational Physics*, Vol. 39, No. 2, 1981, pp. 347-363.
20. Spalart, P. R., "Direct Simulation of a Turbulent Boundary Layer," *J. of Fluid Mechanics*, Cambridge University Press, 1988, 187, pp. 61-98.
21. Guruswamy, G. P., "Computations on Wings with Full-Span Oscillating Control Surfaces using Navier-Stokes Equations," NASA/TM-2013-216601, May 2013.
22. Chan, W. M., "Developments in Strategies and Software Tools for Overset Structured Grid Generation and Connectivity," AIAA Paper 2011-3051, 20th AIAA Computational Fluid Dynamics Conference, June 2011, Honolulu, Hawaii.
23. "Message Passing Interface, MPI," A Message-Passing Interface Standard, University of Tennessee, May 1994.
24. Guruswamy, G. P., "HiMAP: A Portable Super Modular Multilevel Parallel Multidisciplinary Process for Large Scale Analysis," Advances in Engineering Software, Elsevier, Vol. 31, Oct. 2000, pp. 617-620.
25. "OpenMP Application Program Interface," Version 3.1, July 2011. [www.OpenMP.Org, accessed on Nov 22, 2013]
26. "High End Computing Capability," NASA Ames Research Center [http://www.nas.nasa.gov/hecc, accessed on Nov 21, 2013]
27. Guruswamy, G. P., "Large-Scale Computations for Stability Analysis of Launch Vehicles Using Cluster Computers," *J. of Spacecraft and Rockets*, Vol. 48, No. 4, July-Aug. 2011, pp. 584-588.